

An explicit evolution from Néel to striped antiferromagnetic states in the spin-1/2 J_1 - J_2 Heisenberg model on the square lattice

Yun-Tong Yang,^{1,2} Fu-Zhou Chen,^{1,2} Chen Cheng,^{1,2} and Hong-Gang Luo^{1,2,*}

¹*School of Physical Science and Technology & Lanzhou Center for Theoretical Physics, Lanzhou University, Lanzhou 730000, China*

²*Key Laboratory of Quantum Theory and Applications of MoE & Key Laboratory of Theoretical Physics of Gansu Province, Lanzhou University, Lanzhou 730000, China*

The frustrated spin-1/2 J_1 - J_2 Heisenberg model on the square lattice has been extensively studied since 1988 because of its close relationship to the high-temperature superconductivity in cuprates and more importantly involved novel phase of matter in its own right, namely, quantum spin liquid (QSL), one of hot topics in condensed matter physics in recent years. However, the phase diagram of the model, particularly in the maximally frustrated regime $J_2/J_1 \sim 0.5$, is quite controversial, and more seriously the nature of the QSL is not clear at all. Here we provide a pattern picture, on one hand, to show explicitly how the system evolves from the Néel antiferromagnetic (AFM) state at small J_2 to the striped AFM one at large J_2 ; on the other hand, to uncover the nature of the QSL if it exists in the intermediate J_2 coupling regime. For simplicity, we show our results by taking the square lattice $L = L_x \times L_y$ with size $L_x = L_y = 4$ here and periodic boundary condition is considered, and furthermore, exact diagonalization is employed to confirm the correctness of our picture. Our results indicate that the highly frustration regime is characterized by diagonal two-domain, while the Néel AFM state has a diagonal single-domain and the striped AFM state shows itself as a diagonal four-domain, namely, completely diagonal antiferromagnetic order, in the present case. Increasing the system size, the number of the diagonal domains increases correspondingly, but the diagonal single-domain for the Néel AFM state and the diagonal $L_{x(y)}$ -domain for the striped AFM state remain unchanged. Our results shed light on the understanding of the QSL.

Introduction.—Fifty years have passed [1] since the original concept of quantum spin liquid (QSL) has been introduced by Anderson in 1973, called a ‘resonating valence bond’ state formed by firstly pairing spins into singlets and then making a quantum superposition of these singlets at the wavefunction level [2]. The physical importance of the QSL may come from two aspects. The first is that the QSL, in its own right, is a kind of new phase of matter, showing no magnetic orders even in the limit of zero temperature but involving many exotic properties such as non-local excitations, topological nature, and so on. For details, one can refer to some reviews [3–8]. This is obviously beyond the conventional Landau’s paradigm on understanding the phases of matter and their transitions [9–12]. These exotic properties of QSL are believed to hold great potential for quantum communication and computation [13–16]. On the other hand, it was suggested by Anderson in 1987 that high-temperature superconductivity firstly found in cuprates in 1986 [17] might emerge by doping a QSL [18–20]. This is another motivation to explore the nature of QSL because the mechanism of the high-temperature superconductivity remains still open, despite the fact that more and more high-temperature superconducting materials have been found.

However, it indicates that it is actually difficult to make a *positive* answer to the question: what is a QSL? In practice, it usually makes a negative way to identify possible QSLs when neglecting some storied examples (see below). Theoretically, it is popularly believed that a QSL should have a ground state with highly entangled nature, namely, the state is a quantum superposition one, which

cannot be decomposed as a product state by any way through changes of local basis. Although what the highly entangled state looks like or what possible QSLs are have been shown clearly by Kitaev’s toric code model [13] and Kitaev’s honeycomb model [14], respectively, there are no realistic materials to follow completely the physics described by these two models till today. The honeycomb iridate materials were believed to be able to realize the Kitaev-type interaction between neighboring spins [21]. Unfortunately, an additional Heisenberg term is unavoidable due to the direct Ir-Ir overlap and furthermore, this kind of materials are magnetic in nature below certain temperatures [22, 23], which clearly excludes the QSL in these materials. This brings a most popular means to identify candidate materials (models) which might host QSL physics that is to demonstrate experimentally (numerically) the lack of magnetic ordering. This is another negative way to search possible QSLs: what the spins do *not* do. Actually, this is the key difficulty in the study of the QSL physics up to now.

In this work we provide a *positive* attempt to show what the spins do for a given system that is assumed to host a QSL phase. The frustrated spin-1/2 J_1 - J_2 antiferromagnetic Heisenberg model on a square lattice is such an example (J_1 and J_2 are the nearest- and next-nearest-neighbor exchange couplings, respectively). Initial interest in this model was brought from its connection to the high-temperature superconductivity in cuprates [18–20, 24]. It is well-known that this frustrated model is in the Néel AFM state if J_2 is small; otherwise, the model is in the striped AFM phase. But the intermedi-

ate J_2 regime around $J_2 \sim J_1/2$ is still enigmatic [25–42]. Different candidate ground states were proposed by different kinds of methods, including a plaquette valence-bond solid (VBS) state [28, 29, 32, 36, 37], a columnar VBS state [27, 38], a gapless QSL state [34, 35, 39–42] and a gapped QSL state [33]. Even the same method could lead to different conclusions. For example, by using density matrix renormalization group three kinds of phases have been addressed, namely, gapped spin liquid [33], plaquette VBS [36] or gapless spin liquid [39]. Essential difficulties may come from inadequate computational resources and more importantly unclear definition of QSL or indirect evidences such as orders or correlation function behaviors extracted from finite size scaling. Here we employ a pattern picture proposed in our previous works [43–46] to tackle the frustrated spin-1/2 J_1 - J_2 model. Rather successful application of this picture to the one-dimensional (1D) frustrated spin model [46] encourages us to consider this two-dimensional (2D) version of the frustration models and to explore the nature of possible QSL physics in this model.

For the sake of clarity, we take lattice size $L = L_x \times L_y$ ($L_x = L_y = 4$), which is also treated readily with numerical exact diagonalization (ED). The cases with larger lattice sizes are left for the future study. In what follows, periodic boundary condition (PBC) is taken. All spectra of model are readily obtained and the ground state and low-lying excited states can be analyzed in detail. As done previously [46], we firstly diagonalize the Hamiltonian in operator space consisting of spin components at each lattice site, thus obtain six kinds of patterns with high degeneracy (given later). We define domains/kinks along the diagonal orientation for the square lattice, reminiscent of those in the 1D case. The results show that the patterns λ_1 - λ_3 have diagonal single-domain which is identified as Néel AFM pattern and the patterns λ_4 - λ_{15} have diagonal two-domain. The patterns λ_{16} - λ_{21} have diagonal four-domain, identified as striped AFM pattern. With these patterns at hand, we show explicitly how the ground and the first excited states evolve with increasing J_2 : for low J_2 , the patterns λ_1 - λ_3 dominate over the others, and then fade away rapidly; at the same time, the patterns λ_4 - λ_{15} begin to come into play in the intermediate J_2 coupling regime and are suppressed once J_2 increases further; Finally, the patterns λ_{16} - λ_{21} become dominant in the large J_2 regime, and the system enters into the striped AFM phase. Increasing the lattice size, there are more diagonal domains such as two-, four-, six-, \dots , $(L_{x(y)} - 2)$ -domain in the intermediate nonmagnetic regime to come successively into play, and finally the diagonal $L_{x(y)}$ -domain is identified as the striped AFM phase. In the following we provide the detail to confirm our statement.

Model and Method.—The Hamiltonian of the frus-

trated J_1 - J_2 Heisenberg antiferromagnet reads

$$\hat{H}' = J_1 \sum_{\langle i,j \rangle} \hat{\mathbf{S}}_i \cdot \hat{\mathbf{S}}_j + J_2' \sum_{\langle\langle i,j \rangle\rangle} \hat{\mathbf{S}}_i \cdot \hat{\mathbf{S}}_j, \quad (1)$$

where $\langle i,j \rangle$ and $\langle\langle i,j \rangle\rangle$ represent the nearest- and next nearest-neighbor exchange interactions of the spins located at sites i and j , respectively. In what follows, we take J_1 as units of energy and $J_2 = \frac{J_2'}{J_1}$, representing a dimensionless frustration parameter. Thus Eq. (1) is reformulated as $\hat{H}' = \frac{J_1}{2} \hat{H}$, where

$$\hat{H} = \sum_{\langle i,j \rangle} (\hat{\mathbf{S}}_i \cdot \hat{\mathbf{S}}_j + \hat{\mathbf{S}}_j \cdot \hat{\mathbf{S}}_i) + J_2 \sum_{\langle\langle i,j \rangle\rangle} (\hat{\mathbf{S}}_i \cdot \hat{\mathbf{S}}_j + \hat{\mathbf{S}}_j \cdot \hat{\mathbf{S}}_i). \quad (2)$$

Furthermore, Eq. (2) can be written equivalently as a $3L \times 3L$ matrix

$$\hat{H} = \begin{pmatrix} \hat{S}_1^x & i\hat{S}_1^y & \hat{S}_1^z & \hat{S}_2^x & i\hat{S}_2^y & \hat{S}_2^z & \dots & \hat{S}_L^x & i\hat{S}_L^y & \hat{S}_L^z \end{pmatrix} \times \begin{pmatrix} 0 & 0 & 0 & 1 & 0 & 0 & \dots & J_2 & 0 & 0 \\ 0 & 0 & 0 & 0 & 1 & 0 & \dots & 0 & J_2 & 0 \\ 0 & 0 & 0 & 0 & 0 & 1 & \dots & 0 & 0 & J_2 \\ 1 & 0 & 0 & 0 & 0 & 0 & \dots & 0 & 0 & 0 \\ 0 & 1 & 0 & 0 & 0 & 0 & \dots & 0 & 0 & 0 \\ 0 & 0 & 1 & 0 & 0 & 0 & \dots & 0 & 0 & 0 \\ \vdots & \vdots & \vdots & \vdots & \vdots & \vdots & \ddots & \vdots & \vdots & \vdots \\ J_2 & 0 & 0 & 0 & 0 & 0 & \dots & 0 & 0 & 0 \\ 0 & J_2 & 0 & 0 & 0 & 0 & \dots & 0 & 0 & 0 \\ 0 & 0 & J_2 & 0 & 0 & 0 & \dots & 0 & 0 & 0 \end{pmatrix} \times \begin{pmatrix} \hat{S}_1^x & -i\hat{S}_1^y & \hat{S}_1^z & \hat{S}_2^x & -i\hat{S}_2^y & \hat{S}_2^z & \dots & \hat{S}_L^x & -i\hat{S}_L^y & \hat{S}_L^z \end{pmatrix}^T, \quad (3)$$

where the superscript T denotes transpose. This matrix can be diagonalized to obtain eigenvalues and corresponding eigenfunctions $\{\lambda_n, u_n\}$ ($n = 1, 2, \dots, 3L$), which define the patterns marked by λ_n . Thus the J_1 - J_2 Hamiltonian is rewritten as

$$\hat{H} = \sum_{n=1}^{3L} \lambda_n \hat{A}_n^\dagger \hat{A}_n, \quad (4)$$

where each pattern λ_n composes of single-body operators

$$\hat{A}_n = \sum_{i=1}^L \left[u_{n,3i-2} \hat{S}_i^x + u_{n,3i-1} (-i\hat{S}_i^y) + u_{n,3i} \hat{S}_i^z \right]. \quad (5)$$

The validity of Eq. (4) can be confirmed by inserting into the complete basis $|\{S_i^z\}\rangle$ ($i = 1, 2, \dots, L$) with $\hat{S}_i^\pm |\{S_i^z\}\rangle = \pm_i (\uparrow, \downarrow) |\{S_i^z\}\rangle$, as done in Refs.[43–46].

Patterns' Information.—Firstly we explore the properties of the patterns marked by relative signs of eigenfunctions $(u_{n,3i-2}, u_{n,3i-1}, u_{n,3i})$, shown in Fig. 1 and their eigenvalues λ_n as functions of J_2 , given in Fig. 2, from which six kinds of patterns with different degeneracy exist. The first kind of pattern (red line) is threefold-degeneracy which is named the patterns λ_1 - λ_3 . The second one (green line) is twelvefold-degeneracy, named the

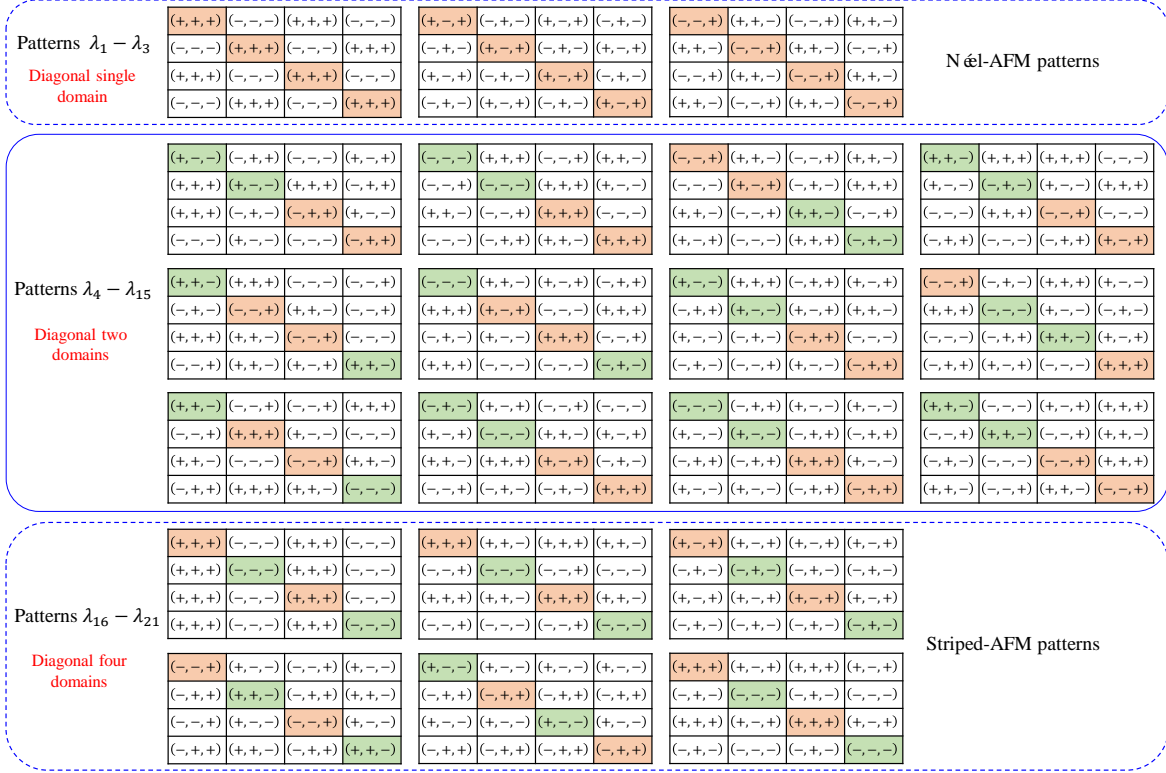


FIG. 1. The patterns and their relative phases obtained by the first diagonalization, marked by the single-body operators Eq. (5) with (\pm, \pm, \pm) denoting the signs of $(u_{n,3i-2}, u_{n,3i-1}, u_{n,3i})$ for the square lattice J_1 - J_2 model with $L = 4 \times 4$ under PBC. The four diagonal sites are marked by orange and green. Orange sites represent $(\pm, \pm, +)$ and green sites represent $(\pm, \pm, -)$. In addition, the patterns' eigenfunctions are free of a total phase factor $e^{i\pi}$ but their relative phases remain fixed.

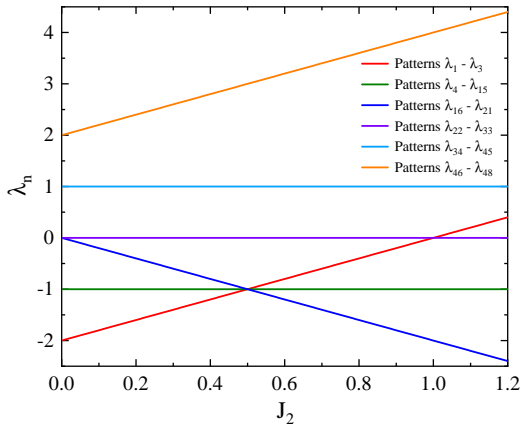


FIG. 2. The eigenenergies of the patterns as functions of the frustrated parameter J_2 for $L = 4 \times 4$ lattice size. Here and hereafter the step of J_2 is taken as 0.003.

patterns λ_4 - λ_{15} and the third one (blue line) is sixfold-degeneracy, named the patterns λ_{16} - λ_{21} . These three kinds of patterns have negative eigenenergies in the most region of the J_2 coupling we consider, thus are impor-

tant to the ground state and the low-lying excited states we are interested in. The remainder is either zero (the patterns λ_{22} - λ_{33}) or positive eigenenergies (the patterns λ_{34} - λ_{45} and λ_{46} - λ_{48}), which have zero or less contribution to the cases we consider here. Therefore, we only list the details in Fig. 1 for first three kinds of patterns.

Here we borrow the concept of magnetic domains/kinks in the 1D spin chain by checking the diagonal direction of square lattice and focus on the domain numbers (due to PBC used, the concept of diagonal domains/kinks behaves well for arbitrary diagonal direction). For each site, there are three spin components S_i^x , $-iS_i^y$ and S_i^z describing the spin state, and we assign the spin z -component to express the spin state and thus other two components represent the dynamical information of the spin at that site. Therefore, we mark the spin states according to the coefficients of S_i^z , i.e. the signs of $u_{n,3i}$. Obviously, the patterns λ_1 - λ_3 have a character of diagonal single-domain and the nearest-neighbor lattices are completely antiferromagnetic for all three components. Thus, the patterns λ_1 - λ_3 are identified as the Néel AFM state. The patterns λ_4 - λ_{15} have a feature of diagonal two-domain, as marked by different colors. The patterns λ_{16} - λ_{21} behave as diagonal four-domain, marked

by alternating colors and a typical striped AFM behavior is obtained. Therefore, the patterns λ_{16} - λ_{21} are identified as striped AFM state.

After the characteristic features of the patterns have been identified, it is interesting to check the corresponding eigenenergies of these patterns, shown in Fig. 2. Obviously, at small J_2 , the patterns λ_1 - λ_3 have lower energies, thus dominate this regime. As a result, this regime is the Néel AFM phase in nature; at large J_2 , the patterns λ_{16} - λ_{21} have lower eigenenergies, which thus dominate this regime by the striped AFM phase; in the intermediate J_2 , i. e. the maximally frustration regime $J_2 \sim J_1/2$, the situation is lightly complicated since this is the regime with a classical high-degenerate point and three kinds of lower-energies patterns compete with each other. In this case, a more careful calculation is needed, as given in the following.

Firstly, one readily obtains the matrix $[\hat{A}_n]_{\{S_i^z\},\{S_i^z\}'} = \langle \{S_i^z\} | \hat{A}_n | \{S_i^z\}' \rangle$ and then Eq. (4) can be solved by diagonalizing the matrix with elements

$$\begin{aligned} \langle \{S_i^z\} | \hat{H} | \{S_i^z\}' \rangle &= \sum_{n=1}^{3L} \lambda_n \\ &\times \sum_{\{S_i^z\}''} [\hat{A}_n^\dagger]_{\{S_i^z\},\{S_i^z\}''} [\hat{A}_n]_{\{S_i^z\}'',\{S_i^z\}'}. \end{aligned} \quad (6)$$

Figure 3 (a1) & (b1) present the results for the ground state and the first excited state energies as functions of J_2 , as shown by thick black solid lines, respectively. In order to confirm the validity of the pattern formulation, the results of direct ED have also presented for comparison, shown as circles. The exact agreement between them from weak to strong J_2 regimes is noticed, which is not surprising since no any approximation has been introduced.

Evolution from Néel to Striped AFM States.—The dissection of the ground state energy is plotted in Fig. 3 (a1), which can be roughly divided into three regions with increasing J_2 . I, the Néel AFM phase, where the patterns λ_1 - λ_3 dominate over others, but the patterns λ_4 - λ_{15} have a remarkable contribution, and even become more and more important. Obviously, this region is somehow different to the standard Néel AFM state due to the presence of the frustration, but we still call it the Néel AFM phase; II, the region that the patterns λ_4 - λ_{15} dominate over others. In this region, the contribution from the patterns λ_1 - λ_3 fades rapidly away and that from the patterns λ_{16} - λ_{21} still grows up. In this case, this region is mainly characterized by the patterns λ_4 - λ_{15} , which have diagonal two-domain in nature, as shown in Fig. 1. The cross point is about $J_{2,c1} \approx 0.363$; III, the striped AFM phase beginning about at $J_{2,c2} \approx 0.635$. In this region, the patterns λ_{16} - λ_{21} dominate over others. These patterns have diagonal four-domain, which are completely

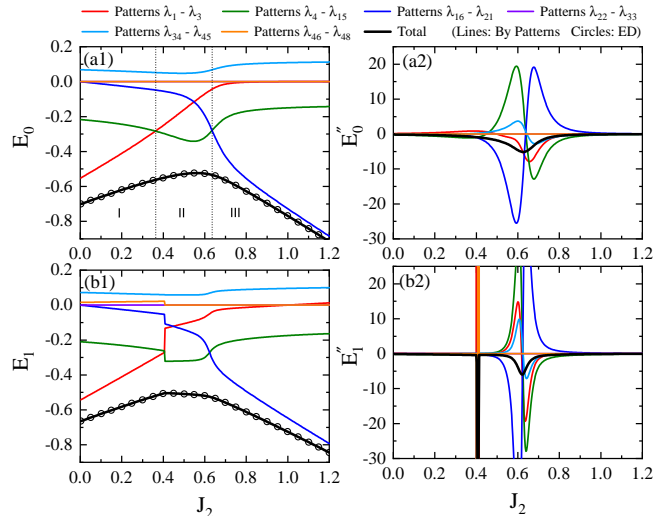


FIG. 3. (a1) & (b1) The ground state and the first excited state energies as functions of the frustration parameter J_2 (thick black solid lines) and their pattern dissections (thin color solid lines). Direct numerical ED (circles) results are also presented to check the validity of the pattern picture. The vertical dashed-lines in (a1) marks two cross points of $J_{2,c1} \approx 0.363$ and $J_{2,c2} \approx 0.635$, respectively, which divide the frustration parameter J_2 into three regions: I, the Néel AFM; II, the diagonal two-domain dominant; and III, the striped AFM. (a2) & (b2) The second derivatives of the corresponding energy levels (thick black solid lines) and their pattern dissections (thin color solid lines).

antiferromagnetic order in the diagonal direction. As a result, the spins form striped structure characterized by the striped AFM state. Still, the contribution from the patterns λ_4 - λ_{15} is prominent, but that from the patterns λ_1 - λ_3 becomes almost zero. In addition, the patterns λ_{34} - λ_{45} have a minor positive contribution due to the interplay between the quantum fluctuation and the magnetic exchange interactions. In addition, other patterns have no contributions to the ground state energy due to either zero pattern energy such as the patterns λ_{22} - λ_{33} or too high pattern energy such as the patterns λ_{46} - λ_{48} .

The above analysis indicates that the pattern energies have a rough correspondence to the actual contributions of the corresponding patterns to the ground state energy, which is specially true in the small and large J_2 regimes since the patterns λ_1 - λ_3 and the patterns λ_{16} - λ_{21} have apparently lower eigenenergies than the others, respectively. However, in the maximal frustration regime, their eigenenergies are comparable, and in particular, are degenerate exactly at $J_2 = J_1/2$, a classical high-degenerate point. The contributions of the patterns to the ground state are mainly determined by the patterns occupancy calculated by $O_0 = \langle \Psi_0 | \hat{A}_n^\dagger \hat{A}_n | \Psi_0 \rangle$ where $|\Psi_0\rangle$ is the ground state wavefunction. Therefore, the distinguished contribution of the patterns λ_4 - λ_{15} to the ground state

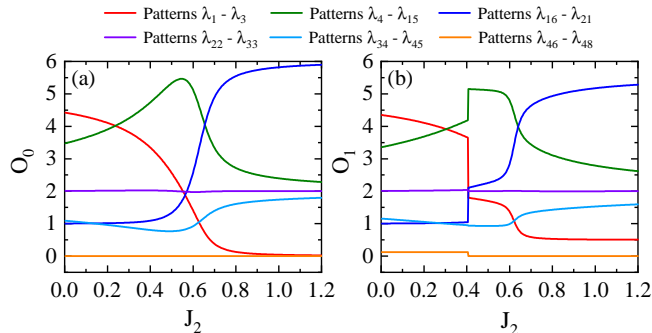


FIG. 4. (a) The patterns' occupancy in the ground state and (b) the first excited state with $L = 4 \times 4$ as functions of J_2 .

comes from that they have large occupancy, as shown in Fig. 4 (a). Thus, the physics of this region is dominated by a diagonal two-domain structure. If a QSL is assumed to exist in this region, the diagonal domain structure is a natural character of the QSL. Surprisingly, these two cross points of $J_{2,c1}$ and $J_{2,c2}$ are roughly consistent with those reported in the literature [31], irrespective of the small lattice size we consider here.

The first excited state has also been analyzed by the same way, as shown in Fig. 3 (b1) and Fig. 4 (b). The contributions of different patterns have similar behaviors, but the first excited state has a first-order phase transition at $J_2 = 0.4$. The phase transition around $J_2 \sim 0.6$ behave more like a continuous one. Figs. 3 (a2) and (b2) provide the second derivative of the ground state and the first excited state energies, which confirm the above statement.

Summary and Discussion.—We use a pattern picture to solve the frustrated spin-1/2 J_1 - J_2 antiferromagnetic Heisenberg model on the square lattice with a small size of $L = 4 \times 4$, which is confirmed by ED result. Our aim is not to solve analytically or numerically this model in a traditional sense, but to explore what the spins do in the maximally frustrated regime, a quite controversial regime, even in the case of large lattice size. On the other hand, this regime is involved an issue of the nature of the QSL if it exists. Our work arrives at this aim, in which a diagonal two-domain structure characterizes this regime, which shed light on the understanding of the QSL in a *positive* sense.

Due to small lattice size, the maximally frustrated regime only dominates by a diagonal two-domain structure. Increasing the lattice size, one can image that there are more domain structures such as diagonal four-, six-, \dots , $(L_{x(y)} - 2)$ -domain to occur, and they will dominate successively the ground state with increasing J_2 . This will be testified for larger lattice size in the future study. In addition, it is also interesting to check other lattice systems like the triangular, honeycomb, Kagomé, and

more, which are useful to further check the nature of the QSL.

Acknowledgments.—The work is partly supported by the National Key Research and Development Program of China (Grant No. 2022YFA1402704) and the programs for NSFC of China (Grant No. 11834005, Grant No. 12174167, Grant No. 12247101).

* luohg@lzu.edu.cn

- [1] S. Kivelson and S. Sondhi, 50 years of quantum spin liquids, *Nature Reviews Physics* **5**, 368 (2023).
- [2] P. Anderson, Resonating valence bonds: A new kind of insulator?, *Materials Research Bulletin* **8**, 153 (1973).
- [3] L. Balents, Spin liquids in frustrated magnets, *Nature* **464**, 199 (2010).
- [4] L. Savary and L. Balents, Quantum spin liquids: a review, *Reports on Progress in Physics* **80**, 016502 (2016).
- [5] Y. Zhou, K. Kanoda, and T.-K. Ng, Quantum spin liquid states, *Rev. Mod. Phys.* **89**, 025003 (2017).
- [6] X.-G. Wen, Colloquium: Zoo of quantum-topological phases of matter, *Rev. Mod. Phys.* **89**, 041004 (2017).
- [7] J. Wen, S.-L. Yu, S. Li, W. Yu, and J.-X. Li, Experimental identification of quantum spin liquids, *npj Quantum Materials* **4**, 12 (2019).
- [8] C. Broholm, R. J. Cava, S. A. Kivelson, D. G. Nocera, M. R. Norman, and T. Senthil, Quantum spin liquids, *Science* **367**, eaay0668 (2020).
- [9] V. Kalmeyer and R. B. Laughlin, Equivalence of the resonating-valence-bond and fractional quantum hall states, *Phys. Rev. Lett.* **59**, 2095 (1987).
- [10] S. A. Kivelson, D. S. Rokhsar, and J. P. Sethna, Topology of the resonating valence-bond state: Solitons and high- T_c superconductivity, *Phys. Rev. B* **35**, 8865 (1987).
- [11] T. Senthil and M. P. A. Fisher, Z_2 gauge theory of electron fractionalization in strongly correlated systems, *Phys. Rev. B* **62**, 7850 (2000).
- [12] J. Knolle and R. Moessner, A field guide to spin liquids, *Annual Review of Condensed Matter Physics* **10**, 451 (2019).
- [13] A. Kitaev, Fault-tolerant quantum computation by anyons, *Annals of Physics* **303**, 2 (2003).
- [14] A. Kitaev, Anyons in an exactly solved model and beyond, *Annals of Physics* **321**, 2 (2006), January Special Issue.
- [15] C. Nayak, S. H. Simon, A. Stern, M. Freedman, and S. Das Sarma, Non-abelian anyons and topological quantum computation, *Rev. Mod. Phys.* **80**, 1083 (2008).
- [16] V. Lahtinen and J. K. Pachos, A Short Introduction to Topological Quantum Computation, *SciPost Phys.* **3**, 021 (2017).
- [17] J. G. Bednorz and K. A. Müller, Possible high T_c superconductivity in the Ba-La-Cu-O system, *Zeitschrift für Physik B Condensed Matter* **64**, 189 (1986).
- [18] P. W. Anderson, The resonating valence bond state in La_2CuO_4 and superconductivity, *Science* **235**, 1196 (1987).
- [19] M. Inui, S. Doniach, and M. Gabay, Doping dependence of antiferromagnetic correlations in high-temperature superconductors, *Phys. Rev. B* **38**, 6631 (1988).
- [20] E. Manousakis, The spin- $\frac{1}{2}$ heisenberg antiferromagnet on

- a square lattice and its application to the cuprous oxides, *Rev. Mod. Phys.* **63**, 1 (1991).
- [21] G. Jackeli and G. Khaliullin, Mott insulators in the strong spin-orbit coupling limit: From heisenberg to a quantum compass and kitaev models, *Phys. Rev. Lett.* **102**, 017205 (2009).
- [22] X. Liu, T. Berlijn, W.-G. Yin, W. Ku, A. Tsvelik, Y.-J. Kim, H. Gretarsson, Y. Singh, P. Gegenwart, and J. P. Hill, Long-range magnetic ordering in Na_2IrO_3 , *Phys. Rev. B* **83**, 220403 (2011).
- [23] S. K. Choi, R. Coldea, A. N. Kolmogorov, T. Lancaster, I. I. Mazin, S. J. Blundell, P. G. Radaelli, Y. Singh, P. Gegenwart, K. R. Choi, S.-W. Cheong, P. J. Baker, C. Stock, and J. Taylor, Spin waves and revised crystal structure of honeycomb iridate Na_2IrO_3 , *Phys. Rev. Lett.* **108**, 127204 (2012).
- [24] X. G. Wen, F. Wilczek, and A. Zee, Chiral spin states and superconductivity, *Phys. Rev. B* **39**, 11413 (1989).
- [25] H. J. Schulz and T. A. L. Ziman, Finite-size scaling for the two-dimensional frustrated quantum heisenberg antiferromagnet, *Europhysics Letters* **18**, 355 (1992).
- [26] H.J. Schulz, T.A.L. Ziman, and D. Poilblanc, Magnetic order and disorder in the frustrated quantum heisenberg antiferromagnet in two dimensions, *J. Phys. I France* **6**, 675 (1996).
- [27] R. R. P. Singh, Z. Weihong, C. J. Hamer, and J. Oitmaa, Dimer order with striped correlations in the J_1-j_2 heisenberg model, *Phys. Rev. B* **60**, 7278 (1999).
- [28] L. Capriotti and S. Sorella, Spontaneous plaquette dimerization in the $j_1 - j_2$ heisenberg model, *Phys. Rev. Lett.* **84**, 3173 (2000).
- [29] M. Mambrini, A. Läuchli, D. Poilblanc, and F. Mila, Plaquette valence-bond crystal in the frustrated heisenberg quantum antiferromagnet on the square lattice, *Phys. Rev. B* **74**, 144422 (2006).
- [30] K. S. D. Beach, Master equation approach to computing rvb bond amplitudes, *Phys. Rev. B* **79**, 224431 (2009).
- [31] J. Richter and J. Schulenburg, The spin-1/2 j_1-j_2 heisenberg antiferromagnet on the square lattice: exact diagonalization for $n=40$ spins, *The European Physical Journal B* **73**, 117 (2010).
- [32] J.-F. Yu and Y.-J. Kao, Spin- $\frac{1}{2}$ J_1-J_2 heisenberg antiferromagnet on a square lattice: A plaquette renormalized tensor network study, *Phys. Rev. B* **85**, 094407 (2012).
- [33] H.-C. Jiang, H. Yao, and L. Balents, Spin liquid ground state of the spin- $\frac{1}{2}$ square J_1-J_2 heisenberg model, *Phys. Rev. B* **86**, 024424 (2012).
- [34] L. Wang, D. Poilblanc, Z.-C. Gu, X.-G. Wen, and F. Verstraete, Constructing a gapless spin-liquid state for the spin-1/2 $J_1 - J_2$ heisenberg model on a square lattice, *Phys. Rev. Lett.* **111**, 037202 (2013).
- [35] W.-J. Hu, F. Becca, A. Parola, and S. Sorella, Direct evidence for a gapless Z_2 spin liquid by frustrating néel antiferromagnetism, *Phys. Rev. B* **88**, 060402 (2013).
- [36] S.-S. Gong, W. Zhu, D. N. Sheng, O. I. Motrunich, and M. P. A. Fisher, Plaquette ordered phase and quantum phase diagram in the spin- $\frac{1}{2}$ J_1-J_2 square heisenberg model, *Phys. Rev. Lett.* **113**, 027201 (2014).
- [37] R. L. Doretto, Plaquette valence-bond solid in the square-lattice J_1-J_2 antiferromagnet heisenberg model: A bond operator approach, *Phys. Rev. B* **89**, 104415 (2014).
- [38] R. Haghshenas and D. N. Sheng, $u(1)$ -symmetric infinite projected entangled-pair states study of the spin-1/2 square J_1-J_2 heisenberg model, *Phys. Rev. B* **97**, 174408 (2018).
- [39] L. Wang and A. W. Sandvik, Critical level crossings and gapless spin liquid in the square-lattice spin-1/2 J_1-J_2 heisenberg antiferromagnet, *Phys. Rev. Lett.* **121**, 107202 (2018).
- [40] F. Ferrari and F. Becca, Gapless spin liquid and valence-bond solid in the J_1-J_2 heisenberg model on the square lattice: Insights from singlet and triplet excitations, *Phys. Rev. B* **102**, 014417 (2020).
- [41] Y. Nomura and M. Imada, Dirac-type nodal spin liquid revealed by refined quantum many-body solver using neural-network wave function, correlation ratio, and level spectroscopy, *Phys. Rev. X* **11**, 031034 (2021).
- [42] W.-Y. Liu, S.-S. Gong, Y.-B. Li, D. Poilblanc, W.-Q. Chen, and Z.-C. Gu, Gapless quantum spin liquid and global phase diagram of the spin-1/2 j_1-j_2 square antiferromagnetic heisenberg model, *Science Bulletin* **67**, 1034 (2022).
- [43] Y.-T. Yang and H.-G. Luo, Dissecting Quantum Phase Transition in the Transverse Ising Model, arXiv e-prints , arXiv:2212.12702 (2022).
- [44] Y.-T. Yang and H.-G. Luo, First-Order Excited-State Quantum Phase Transition in the Transverse Ising Model with a Longitudinal Field, arXiv e-prints , arXiv:2301.02066 (2023).
- [45] Y.-T. Yang and H.-G. Luo, Pattern Description of Quantum Phase Transitions in the Transverse Antiferromagnetic Ising Model with a Longitudinal Field, arXiv e-prints , arXiv:2301.05040 (2023).
- [46] Y.-T. Yang and H.-G. Luo, Pattern description of the ground state properties of the one-dimensional axial next-nearest-neighbor Ising model in a transverse field, arXiv e-prints , arXiv:2301.08891 (2023).